Title: α-Synuclein facilitates clathrin assembly in synaptic vesicle endocytosis

Short title: α-Synuclein regulates clathrin assembly

Karina J Vargas[1*#], P. L. Colosi[1,2*#], Eric Girardi[1*], Sreeganga S Chandra[1,3]

[1] Departments of Neurology; Neuroscience, Yale University, New Haven, CT 06536
[2] PREP Program, Yale University, New Haven, CT 06511
[3] To whom correspondence should be addressed to:
sreeganga.chandra@yale.edu ; 203-785-6172

*Authors contributed equally to this study
Present Address:
KJV, Marine Biological Laboratory, MA
PLC, University of Pennsylvania, PA

Summary (40 word limit): Synucleins can sense and generate membrane curvature. We previously showed that synuclein null mice exhibit deficits in synaptic vesicle endocytosis. Here, Vargas et al. provide evidence that α-synuclein functions specifically in clathrin assembly during early steps of synaptic vesicle endocytosis.

Abstract (160 word limit):

α-Synuclein plays a central role in Parkinson's disease (PD); hence, elucidating its normal physiological function(s) is important. α-Synuclein and family members β-, and γ-synuclein, are presynaptically enriched proteins. Synucleins sense and generate membrane curvature, properties consistent with their described roles in synaptic vesicle (SV) cycling. We have previously shown SV endocytosis (SVE) deficits in αβγ-synuclein knockout (KO) neurons. Here, we investigate which steps of SVE are regulated by α-synuclein. Immuno-electron microscopy (EM) of synaptosomes reveals that α-synuclein relocalizes from SVs to the synaptic membrane upon stimulation, allowing α-synuclein to function there during or after stimulation. Using membrane recruitment assays, we show that α-synuclein is co-localized with clathrin patches. We also observe that recruitment of clathrin and its adaptor, AP180, to synaptic membranes is altered in the absence of synucleins. Visualizing clathrin assembly on membranes in an *in vitro* reconstitution system reveal that synucleins increase clathrin patch size and curvature, facilitating clathrin coated pit maturation during the early steps of SVE.

Introduction

α-Synuclein became a principal focus of neurodegenerative research when it was identified as the major constituent of Lewy Bodies, the pathological protein aggregates found in the brains of PD patients [1]. The importance of α-synuclein was further underscored by the identification of families with Mendelian forms of PD arising from causal point mutations and gene multiplications of *SNCA*, the α-synuclein gene [2-7]. Genome-wide association studies have shown that sequence variants in *SNCA* are also associated with sporadic PD [8, 9]. Based on these observations, many current therapeutic strategies for PD are focused on eliminating or reducing α-synuclein levels in the brain. Therefore, there is a growing interest in understanding α-synuclein's physiological functions and how loss of α-synuclein impacts neuronal functions.

Since its discovery as a SV-associated protein in the electric organ of *Torpedo* [10], several distinct approaches have been used to determine the physiological function(s) of α-synuclein. Structural studies have revealed that α-synuclein can adopt several conformations, principally, unfolded in solution, but also α-helical on phospholipid membranes. In α-helical conformations, the N-terminus folds into either a single elongated amphipathic helix on flatter membranes or a 'broken' helix when bound to curved lipid membranes [11, 12]. α-Synuclein can switch between the two membrane conformations but has a

stronger affinity for highly curved membranes [13]. These biophysical properties are shared by β-, and γ-synuclein. The conformational plasticity of synucleins allows these proteins to sense and generate membrane curvature.

The initial finding in *Torpedo*, itself suggested an α-synuclein function related to SV trafficking. The membrane-bending properties of synucleins suggest that they regulate SV exocytosis and/or endocytosis. Biochemical studies have indicated a role for α-synuclein in exocytosis [14, 15]. For instance, α-synuclein has been shown to interact with synaptobrevin2, a v-SNARE protein required for SV fusion [15-17]. Somewhat surprisingly, electrophysiological studies suggest that neurotransmission is normal or even improved in αβγ-synuclein KO mice [15, 18, 19], raising questions about the relevance of this interaction for exocytosis. Other studies have convincingly demonstrated α-synuclein's role in modulating SV mobilization and recycling, specifically in SVE [20, 21]. Additionally, analysis of dense core vesicles (which have larger diameter than SVs) in synuclein KOs suggest a role in fusion pore expansion [22]. Taken together, the preponderance of functional studies supports synucleins acting post-fusion, in SVE, and in SV clustering [23].

Through pHluorin imaging and cholera toxin labelling, we determined that αβγ-synuclein KO hippocampal neurons exhibit slower kinetics of SVE [20]. Consistently, our unbiased proteomics of synaptosomes from αβγ-synuclein KO mice show significant changes in SVE proteins: increases in clathrin and endophilins and a decrease in levels of the v-SNARE adaptor protein AP180 (neuronal homolog of CALM) [18, 20, 24]. Recent proteomic analyses of α-synuclein-interacting proteins using proximity labelling in cortical neurons revealed SVE as one of the most robustly represented pathways [25]. In addition, we have shown that the interaction between α-synuclein and synaptobrevin2 observed by other researchers [15, 16, 26] is part of a larger complex of which AP180 is a major component [20]. AP180 along with AP2 are the main recruiters of clathrin to synaptic membranes and act to initiate clathrin coated pit (CCP) formation. These adaptors are critical for both clathrin assembly and SV protein sorting [27-30]. This suggests that the transient α-synuclein-AP180-synaptobrevin2 complex may play a role post-fusion in SV protein retrieval.

Building on our previous finding of slowed SVE in αβγ-synuclein KOs, we aimed to identify which step(s) of SVE are regulated by synucleins. We compared the ultrastructural features of endocytic mutant synapses to those seen in αβγ-synuclein KOs [18, 20, 21]. AP180 KO mice exhibit a higher density of vesicles [27] similar to αβγ-synuclein KOs [18]. Dynamin1, endophilins, synaptojanin1, and auxilin that regulate later stages of endocytosis, such as CCP curvature generation, scission and uncoating, when deleted show striking synaptic ultrastructural phenotypes. Dynamin1 KO synapses are unable to scission CCPs to generate clathrin coated vesicles (CCVs) [31, 32]–consequently, presynaptic termini become filled with endocytic tubules decorated with CCPs [33]. Contrastingly, endophilin, synaptojanin1, and auxilin KO synapses feature

accumulations of CCVs, due to impaired CCV uncoating. αβγ-synuclein KO synapses did not display any of the morphological abnormalities observed–endocytic tubules with CCPs or CCVs–when later stages of SVE are blocked [20]. This suggests α-synuclein's participation in an earlier stage of SVE similar to AP180.

Here, we performed a wide range of *in vitro* experiments to test whether α-synuclein modulates clathrin recruitment through its membrane bending properties and interactions with other proteins. We visualized α-synuclein's subcellular localization, monitored clathrin polymerization on the membrane, and determined how clathrin structures are altered by the presence or absence of α-synuclein. In a minimal reconstitution system, we show that clathrin cage formation is affected by the addition of recombinant α-synuclein. These experiments collectively demonstrate that the locus of α-synuclein action in SVE is clathrin assembly.

Results and Discussion

The localization of α-synuclein within synapses is dynamic

The majority of α-synuclein is found on SVs at rest [21, 34], consistent with its preference to bind highly curved membranes [35, 36]. To determine whether the localization of α-synuclein is changed upon synaptic stimulation, we prepared fresh synaptosomes from wildtype mouse brains, and tested three physiological conditions: rest, depolarization with high K^+, and repolarization. The synaptosomes were then embedded in agarose, fixed, immunolabelled with an α-synuclein or synaptobrevin2-specific antibody and imaged using EM. At rest, the majority of α-synuclein is present on SVs (61.1% on SVs, 25.9% on membranes; 5.9% in cytosol; **Fig 1A**, **B**), similar to the integral SV protein synaptobrevin2 (78.2% on SV, 12.0% on membranes, 3.1% in cytosol; **Fig 1A**, **C**). These data are in line with previous publications [21]. Interestingly, upon stimulating synaptosomes with high K^+, α-synuclein relocates from SVs to the synaptic plasma membrane and cytosol (30.1% on SVs, 51.1% on membranes, 11.2% in the cytosol; Rest versus K^+ stimulation: 61.1% versus 30.1% on SVs; $p<0.001$). Our results are congruent with previous confocal imaging, which showed α-synuclein becoming diffuse upon neuronal stimulation [37, 38]. As expected, synaptobrevin2 remains mainly on SVs when stimulated (Rest versus K^+ stimulation: 78.2% versus 68.4% on SVs; $p= 0.095$). Repolarization leads to relocalization of α-synuclein on SVs (70.1% on SVs, 18.2% on membranes, 3.8% in cytosol). To validate these results, we measured the distance from the gold particle to the nearest SV. The distances measured for α-synuclein at rest, high K^+, and repolarization were 7.73 nm, 11.32 nm and 4.61 nm, while those for synaptobrevin2 were 10.22 nm, 9.47 nm, and 8.8 nm, respectively. Thus, the sub-synaptic location of α-synuclein is dynamic and is likely to be linked to the SV cycle.

Localization of α-synuclein to the synaptic plasma membrane upon neuronal stimulation strongly supports that α-synuclein functions during SV endocytosis. To confirm this, we examined the location of α-synuclein in dynamin1,3 double KO synapses, which feature few SVs and large CCP-

158 decorated invaginations of the synaptic plasma membrane. This leads to the
159 capture of SVE proteins in CCPs, visualized as their apparent clustering in
160 confocal images. While exocytic and peripheral SV proteins, such as rab3a and
161 synapsin, appear unchanged or diffuse, respectively [33, 39]. Immunostaining of
162 dynamin1,3 double KO neurons revealed that α-synuclein behaves as an
163 endocytic protein, clustering and co-localizing with clathrin and other endocytic
164 proteins (**Fig. S1**). This is consistent with our previous findings [20] and suggests
165 that α-synuclein is an accessory endocytic protein that functions prior to dynamin
166 recruitment.
167
168 **α-Synuclein co-localizes with a fraction of clathrin patches**
169 In order to visualize if α-synuclein co-localizes with clathrin patches at early
170 stages of clathrin mediated endocytosis, we used a sheared membrane sheet
171 preparation. Membrane-GFP transfected PTK2 cells were grown on coverslips and
172 briefly sonicated to unroof the cells, leaving behind adherent membranes. These
173 coverslips were washed and incubated with cytosol prepared from wildtype mouse
174 brain and GTPγS (to prevent dynamin function) with an ATP generation system for
175 increasing amounts of time (t=0-30 minutes). The membranes were then
176 immunostained for clathrin and α-synuclein to visualize their distribution on the
177 membrane sheets. As seen in **Fig. 2A-C**, at t=0, both clathrin and α-synuclein are
178 present in puncta on the membranes. Strikingly, some puncta contain both proteins
179 in the distinct pattern of a clathrin patch with α-synuclein colocalized at its inner
180 core (**Fig. 2B**). We measured fluorescence intensity and size of clathrin and α-
181 synuclein patches for each punctum. We plotted all puncta (n=2071) observed by
182 their relative clathrin and α-synuclein fluorescence and binned them in 5 size
183 categories based on the diameter of clathrin patches (**Fig. 2D**). When these data
184 were plotted as a function of clathrin diameter (**Fig. 2E**), for a given clathrin puncta
185 size, the average clathrin fluorescence exceeded that of α-synuclein, suggesting
186 that α-synuclein is found within clathrin patches and not the other way around. As
187 expected, average clathrin fluorescence increases linearly with puncta size.
188 However, average α-synuclein fluorescence is largely constant and only increases
189 in very large patches (diameter > 1.6 μm) (**Fig. 2E**, blue and purple). This indicates
190 that α-synuclein can colocalize with clathrin, predominantly in large puncta.
191
192 To classify the puncta into clathrin only, α-synuclein only, and clathrin+α-synuclein
193 puncta, we set cutoffs at x=0.5 and y=1 (**Fig. 2D**). Using these cutoffs, 21% of
194 puncta were positive for both proteins, 59% for clathrin only, 20% for α-synuclein
195 only (**Fig. 2G**; t=0). The average diameters α-synuclein only, clathrin only, and
196 clathrin+α-synuclein puncta were 0.53 μm, 0.66 μm, and 0.96 μm, respectively
197 (**Fig. 2F**; n=1174, p=0.001), indicating that clathrin+α-synuclein puncta are
198 consistently larger than clathrin only puncta.
199
200 Next, we tested how the distribution and size of the 3 classes of puncta (α-
201 synuclein only, clathrin only, and clathrin+α-synuclein) change over time (0, 5, 15,
202 30 minutes) during incubation with brain cytosol (**Fig. 2F, S2A**). Interestingly, we
203 observe that the fraction of clathrin only puncta decreases (59% at t=0 to 0% at

t=30) with a concomitant increase in clathrin+α-synuclein puncta (20% at t=0 to 50% at t=30), indicating that α-synuclein and clathrin might be co-assembling (**Fig. 2G**, **S2B**). The average size of α-synuclein only and clathrin only puncta remain constant, while that of clathrin+α-synuclein puncta diameter changes over time (**Fig. 2F**, **S2A**; 0.96 μm at t=0 and 0.77 μm at t=30), mirroring the dynamics of clathrin+α-synuclein puncta. It is known that incubation with brain cytosol (t=30 minutes) leads to the growth and curvature of the clathrin lattice to form mature CCPs that are ready to be scissioned [40]. So, at this time point, clathrin+α-synuclein puncta may represent these structures.

To test if clathrin and α-synuclein co-localize on synaptic membranes, we purified synaptosomes from the brains of wildtype and αβγ-synuclein KO mice. We identified proteins in close proximity to α-synuclein, by treating the synaptosomes with a membrane permeable crosslinker, and the crosslinked proteins were then immunoprecipitated with an α-synuclein antibody (**Fig. S3**). Unique bands of immunoprecipitated proteins from wildtype samples were processed for mass spectroscopy. The αβγ-synuclein KO samples served as a negative control to identify non-specific interactions. This unbiased analysis revealed that clathrin heavy chain was present in wildtype samples but absent in the αβγ-synuclein KO samples (**Fig. S3**), indicating that events observed on PTK2 membranes might also occur on synaptic membranes.

Membrane recruitment of endocytic proteins is altered by the lack of synucleins

To interrogate α-synuclein involvement in endocytic protein recruitment to the synaptic membrane, we performed an *in vitro* protein recruitment assay. Stripped synaptic membranes isolated from wildtype mouse brain were incubated with cytosol obtained from wildtype or αβγ-synuclein KO mouse brains. αβγ-synuclein KO mouse brains show compensatory increases in clathrin, endophilin, and synapsins, decreases in AP180 levels and altered AAK1 splicing (**Fig. 3**; [20]). The incubations were supplemented with an ATP generation system and GTPγS similar to the PTK2 membrane experiments (**Fig. 2**). As a positive control, we used synapsin, whose levels are increased in αβγ-synuclein KO and known to bind synaptic membranes [41] (**Fig. 3**). As expected, synapsin binds membranes in proportion to its expression. In the same fashion, we found increased recruitment of clathrin heavy and light chains when synucleins are absent from the cytosol (1.6 ± 0.2 fold, p=0.0061 for clathrin heavy chain; 3.4 ± 0.4 fold, p=0.0016 for clathrin light chain; **Fig. 3**), largely reflecting the increased clathrin levels in the αβγ-synuclein KO cytosol [18, 42]. Fascinatingly, we observed increased AP180 recruitment (1.4 ± 0.1 fold, p=0.033), despite decreased AP180 levels in αβγ-synuclein KO cytosol [20]. We then calculated the clathrin:AP180 ratio on synaptic membranes and determined it was also increased in αβγ-synuclein KOs (1.14-2.42 fold for heavy and light chain, respectively).

Other key endocytic proteins were tested in the membrane recruitment assay with no significant results. These include AP-2, FBP17, epsin1, Eps-15,

250 AAK1, endophilin-A1, necap and dynamin1, all proteins that function in SVE. We
251 also did not observe altered recruitment of Rab3. Based on these findings, we infer
252 that synucleins may modulate recruitment of clathrin and AP180, proteins involved
253 in the initiation of SVE.
254
255 **Lipid monolayer assay to investigate clathrin assembly**
256 Our previous SVE kinetic measurements [20] showed slower endocytosis
257 in αβγ-synuclein KO neurons and now we observe increased membrane
258 recruitment of clathrin and AP180 *in vitro* (**Fig. 3**). Therefore, we sought to
259 determine the state of clathrin assembly on the membrane. Also, as the
260 clathrin:adaptor ratio is one determinant of CCP curvature [43], we wanted to test
261 if the increased clathrin:AP180 ratio seen in the αβγ-synuclein KO condition
262 indicates shallower CCPs.
263
264 In order to visualize clathrin assembly, lipid monolayer assays (**Fig. 4A**)
265 designed for purified proteins were adapted for brain cytosol [30], and EM was
266 performed (**Fig. 4B**). The assays were performed with wildtype and αβγ-synuclein
267 KO cytosol and the time dependence of clathrin assembly into flat lattices and
268 mature CCPs was quantified. We established that incubation of the lipid monolayer
269 with wildtype cytosol leads to assembly of flat and curved clathrin lattices, with a
270 typical hexagonal pattern by 15 minutes (**Fig. 4B**, **C**), in line with previous
271 publications [30]. On occasion, mature CCPs were also seen (**Fig. 4B**). The size
272 of individual clathrin patches were quantified. As seen in **Fig. 4**, absence of
273 synucleins initially leads to significantly smaller clathrin patches (**Fig. 4C**, t=15,
274 wildtype (WT)= 30,808 ± 2,617 nm^2 and αβγ-synuclein KO (TKO)= 25,544 ± 2,134
275 nm^2, $p<0.001$), but by t=23 minutes, the patches are significantly larger (t=23, WT=
276 36,513 ± 2597 nm^2, and TKO= 64,882 ± 3790 nm^2, $p<0.05$). Thus, there is delayed
277 clathrin assembly in the αβγ-synuclein KO, consistent with the functional data in
278 hippocampal neurons [20]. Since increased clathrin:adaptor ratio is associated
279 with decreased CCP curvature, we examined the curvature of clathrin patches by
280 analyzing the fraction of pentagons and heptagons per hexagons in the clathrin
281 formations (**Fig. 4D**, **E**). The presence of pentagons and/or heptagons indicates
282 that a curved lattice is being generated. We find that incubation with αβγ-synuclein
283 KO cytosol leads to fewer non-hexagonal clathrin formations (**Fig. 4E**, **F**),
284 indicating flatter clathrin lattices.
285
286 To confirm that clathrin assembly deficits are caused by the absence of
287 synuclein, we performed rescue experiments, by adding to the αβγ-synuclein KO
288 cytosol, recombinant mouse α-synuclein matched to the amount in wildtype brain
289 cytosol. Addition of mouse α-synuclein to the αβγ-synuclein KO cytosol rescued
290 both the kinetics and the formation of enlarged clathrin patches, at later time points,
291 to that of wildtype sizes (t=30, WT= 54,434 ± 3,165 nm^2, TKO= 81,753 ± 5,840
292 nm^2, and TKO + α-synuclein= 58,510 ± 4,127 nm^2; WT versus TKO + α-synuclein,
293 ns) (**Fig. 4B**, **C**). In addition, there was a greater number of lattices with pentagons
294 and heptagons, which are associated with curved lattices (**Fig. 4E**, **F**). Together,

these results strongly suggest that synucleins function to assemble clathrin and curve the lattice.

To unequivocally establish α-synuclein's role in clathrin assembly on the membrane, we performed the lipid monolayer assay (**Fig. 4A**) using purified proteins in place of cytosol (**Fig. 5A**). Addition of clathrin has no observable effect on membranes due to its inability to directly bind them (**Fig. 5B**), while AP180 can bind the lipid monolayer and modestly deform it (**Fig. 5B**). Injection of recombinant mouse α-synuclein only leads to membrane ruffles and deformations (**Fig. 5C**) consistent with its ability to bend membranes. The addition of both AP180 and clathrin leads to the formation of discrete cages (**Fig. 5D**), confirming previous literature that AP180 is both necessary and sufficient for CCP and clathrin lattice formation [30]. Further, addition of α-synuclein leads to significantly larger clathrin assemblies (**Fig. 5D, E**) (Clathrin+AP180 = 8607 ± 413 nm^2, Clathrin+AP180+α-synuclein= 15,569 ± 2131 nm^2; $p<0.01$). We were unable to determine the non-hexagon/hexagon ratio for these images, due to the irregularity of the lattices as well as the high contrast needed to view these structures. However, we find that addition of clathrin, AP180 and α-synuclein leads to the formation of juxtaposed CCPs, congruent with membrane curvature generation.

Discussion

α-Synuclein has been implicated in several steps of the synaptic cycle. Here we expound on efforts to elucidate precise mechanisms by which synucleins regulate SVE. Our results strongly suggest that the observed slower endocytosis of SVs in αβγ-synuclein KO neurons is due to impairment of clathrin assembly and curvature generation on synaptic membranes.

Synucleins are accessory endocytic proteins

Our findings on α-synuclein add to a growing body of work identifying synucleins as endocytic accessory proteins. First, the biophysical properties of synucleins are similar to those of SVE proteins. Synucleins bind acidic lipids, especially $PI(4,5)P_2$, a feature of many endocytic proteins. Synucleins are effective membrane curvature sensors and generators. The ability to bend membranes is an important property of many early SVE proteins. Second, α-synuclein is recruited to the synaptic membrane, the locus of SVE. As shown in **Fig. 1**, α-synuclein is dynamic and relocalizes to the synaptic membrane upon stimulation, allowing it to participate in post-fusion events such as SVE. Other SVE proteins such as AP2, endophilins, and dynamin behave in a similar manner [44-46]. Moreover, in dynamin1,3 double KO neurons where SVE proteins are trapped in CCPs that do not resolve, α-synuclein is clustered with other endocytic proteins (**Fig. S2**). α-Synuclein's behavior in dynamin1,3 double KO differs from those of other peripheral SV proteins like synapsin and rab3a (**Fig. S2**). Third, the known proteins that interact with α-synuclein also support a role in SVE. α-Synuclein can multimerize on membranes, forming patches (**Fig. 2C**). Further, unbiased proximity labelling [25] and crosslinking suggest that clathrin (**Fig. S3**) and other SVE proteins are *in situ* binding partners on the membrane [25]. These interactions

are of low affinity and multivalent, similar to other SVE protein interactions. Finally, the absence of synucleins leads to slowed SVE and enhanced frequency depression due to decreased SV pool recovery [20]. In this study, we present a preponderance of evidence that α-synuclein functions in clathrin assembly.

One striking finding in our study is that α-synuclein localizes to the center of clathrin patches (**Fig. 2**). A systematic survey of the sub-cellular localization of endocytic proteins in clathrin assembled structures has been published on HeLa cell sheets. [47]. This work was performed using correlative super resolution microscopy combined with electron microscopy and beautifully showed that most endocytic proteins are found at the edge of clathrin assemblies (both flat lattices and CCPs were evaluated) on the membrane. The only two proteins always found in the middle of the clathrin structures were CALM and VAMP, the non-neuronal homologs of AP180 and synaptobrevin2 [47]. Together with our finding, the results of these studies suggest that α-synuclein is localized with AP180 and synaptobrevin2 at the center of the patch. It is tempting to speculate that this serves to achieve the high number of synaptobrevin2 molecules present on the SV (~31/SV). In support for this idea, SVs purified from αβγ-synuclein KO brains show lower levels of synaptobrevin2 compared to WT brains [20]. Similarly, in AP180 KO mice, activity-dependent defects in synaptobrevin2 recycling resulting in reduced synaptobrevin2 levels on SVs have been observed [29].

What does α-synuclein do in CCP formation? Since clathrin is unable to directly bind membrane, its recruitment requires adaptor proteins that bind both clathrin and the membrane. Besides adaptors, accessory and regulatory endocytic proteins are required for effective clathrin recruitment. α-Synuclein falls into this category of proteins. Via its multi-valent interactions with PI(4,5)P2, [15, 16, 20, 26] and its ability to self-assemble on the membrane (**Fig. 2C**), and bend it (**Fig. 5C**), α-synuclein can regulate the binding of AP180 to the membrane (**Fig. 3A**, **C**), thereby promoting clathrin patch initiation. This is supported by our previous finding that α-synuclein and AP180 are part of a transient protein complex that assembles post-stimulation [20]. Our present direct observation of α-synuclein within larger clathrin patches on cell membranes (**Fig. 2B**), and that addition of α-synuclein to purified AP180 and clathrin in the lipid monolayer assay leads to bigger clathrin patches (**Fig. 5D-E**) are also in line with this premise. Interpreting the results from the αβγ-synuclein KO experiments is complicated by the compensatory changes in the cytosolic levels of clathrin and AP180 (**Fig. 3A**, **C**) and phosphorylation changes in endocytic proteins [21]. Yet, the time course of clathrin lattice formation is initially slower mirroring the slow kinetics of SVE (**Fig. 4B-C**) [20]. The larger patches seen with the αβγ-synuclein KO cytosol at later time points (**Fig. 4C**) likely occurs due to the upregulated levels of clathrin in the αβγ-synuclein KO cytosol (**Fig. 3A**, **C**). We speculate that the larger clathrin patches take longer to fully curve also contributing to the decreased rate of SV endocytosis [20]. Congruently, we do find CCPs with fewer pentagons and heptagons in the αβγ-synuclein KO condition in the lipid monolayer assays (**Fig. 4E**). In the rescue condition, the clathrin patch size is restored (**Fig. 4C**) despite more clathrin in the cytosol, because the resulting

387 patches are more curved (**Fig. 4E-F**). Thus, α-synuclein appears to coordinate
388 clathrin assembly with curvature generation.
389
390 **α-Synuclein, SVE and PD**
391 Significantly, both transgenic and acute overexpression models of α-synuclein that
392 replicate triplication of the α-synuclein PD locus (PARK4) show impairment of SVE
393 [48-51]. Thus, both deletion and overexpression of α-synuclein lead to a similar
394 endocytic phenotype. This indicates that SVE is sensitive to levels of α-synuclein.
395 In the overexpression models, α-synuclein is likely to impact several steps of SVE.
396 In addition to any possible disruption of clathrin assembly on the membrane, α-
397 synuclein is also likely to impact the uncaging of CCVs. Indeed, injection of α-
398 synuclein in the giant Lamprey synapse leads to an accumulation of both CCPs
399 and CCVs [48]. The uncoating of CCVs is regulated by the heat shock protein
400 Hsc70 and its co-chaperone auxilin. Hsc70 has been shown to bind both unfolded
401 monomeric α-synuclein and α-synuclein fibrils, thus excess α-synuclein is likely to
402 sequester available Hsc70 from the uncoating reaction [52]. Interestingly, loss-of-
403 function mutations in both auxilin and the PIP phosphatase synaptojanin1 that
404 function in CCV uncoating cause familial PD [53-56]. Thus, SVE is a key pathway
405 in the pathogenesis of PD.
406
407
408 **Materials and Methods**
409
410 **Immuno-electron microscopy of mouse brain synaptosomes:**
411 *Synaptosome Isolation*
412 Brains from Wildtype mice (n=3) were harvested and washed in homogenizing
413 buffer (0.32 M Sucrose, 10 mM Tris-HCl pH 7.4, mini cOmplete protease inhibitor
414 tablet). Cerebella were removed, hemispheres separated, and white matter
415 removed before adding the remaining brain to 10 mL of homogenizing buffer.
416 Brains were homogenized in a 55 mL Potter homogenizer at 80% power for 8
417 strokes. Homogenate was centrifuged at 2,330 x g for 4 min at 4°C in a JA-20
418 rotor. Pellet (P1) was discarded and supernatant (S1) was transferred to a 50 mL
419 centrifuge tube. S1 was recentrifuged at 18,850 x g for 12 min at 4°C. Supernatant
420 (S2) was discarded and pellet (P2) was resuspended in 6 mL of homogenizing
421 buffer. Gradients of Percoll solutions (from bottom to top: 2.5 mL 23%, 3 mL 10%,
422 and 2.5 mL 3%) were prepared in 15 mL glass tubes. 2 mL of resuspended P2
423 was added to the top of each gradient, and tubes were centrifuged at 18,850 x g
424 for 12 min at 4°C. Synaptosome fractions were collected by Pasteur pipette.
425
426 *Stimulation*
427 Washing buffer Krebs 1 (140 mM NaCl, 10 mM Tris-HCl pH 7.4, 5 mM KCl, 5 mM
428 $NaHCO_3$, 1.3 mM $MgSO_4$, 1 mM Na-phosphate buffer) was added to the collected
429 synaptosomes, and sample was centrifuged at 18,850 x g for 12 min. Pellet was
430 resuspended in 1.5 mL Krebs 1 and divided equally into three 1.5 mL
431 microcentrifuge tubes labeled for rest, stimulation, and recovery. The tubes were
432 centrifuged at 16,000 x g for 3 min. Each pellet was resuspended in 500 μL of

433 washing buffer Krebs 2 (10 mM glucose, 1.2 mM CaCl2 in Krebs 1) and incubated
434 in a 37°C water bath for 15 min. The rest condition was left in the bath while the
435 stimulation and recovery conditions were each removed, supplemented to 90 mM
436 KCl final concentration, rotated by hand, and returned to the bath for 2 min.
437 Stimulation and recovery tubes were then spun at 16,000 x g for 2 min. The
438 stimulation pellet was resuspended in 200 μL Krebs 1 and left on ice. The recovery
439 pellet was resuspended in 500 μL of washing buffer Krebs 3 (10 mM Glucose, 1
440 mM EGTA, 1 phosSTOP tablet in Krebs 1) and returned to the bath for 10 min.
441 The recovery and rest tubes were removed from the bath and spun at 16,000 x g
442 for 2 min. Pellets were resuspended in 200 μL of Krebs 1. All conditions were
443 transferred into separate 50 mL centrifuge tubes filled with 30 mL of hypotonic
444 fixative solution (3% paraformaldehyde, 0.25% glutaraldehyde in 5 mM Na-
445 phosphate buffer) and incubated on ice for 30 min.
446
447 *Agarose Embedding*
448 The samples were centrifuged in their 50 mL tubes at 18,850 x g at 4°C for 12 min.
449 Each pellet was resuspended in 400 μL of 120 mM Na-phosphate buffer. 180 μL
450 aliquots of each sample were pipetted into glass test tubes and held on ice until
451 mixed with agarose. Pasteur pipettes and glass slide frames (see [57]) were
452 warmed in a 60°C oven. 3% Agarose solution was prepared in 5 mM Na-phosphate
453 buffer, warmed to 95°C until agarose dissolved, and kept in a 54°C water bath.
454 180 μL of agarose solution was pipetted over each broken synaptosome sample
455 while the tube was held in the 54°C water bath and mixed by gentle pipetting with
456 a Pasteur pipette. The agarose-embedded samples were pipetted into the warmed
457 glass slide frames and solidified on ice. Once solid, the frames were disassembled,
458 leaving a solid agarose gel sheet on one glass slide. The gel was cut into 3 mm^3
459 cubes with a razor blade and washed from the slide with 120 mM Na-phosphate
460 buffer into petri dishes.
461
462 *Immunolabeling and Electron Microscopy Preparation*
463 Each condition's cubes were divided into 5 wells of glazed porcelain well plates.
464 Cubes were incubated for 30 min with 5% bovine serum albumin (BSA) in solution
465 A (0.5 M NaCl, 0.02 M Na-phosphate buffer) at room temperature. BSA solution
466 was removed and each well was incubated overnight with 200 μL of primary
467 antibodies in solution A at 4°C. Cubes were washed with 5 changes of solution A
468 over the course of 1.5 hours. Solution A was removed from the wells and cubes
469 were incubated with secondary antibodies in solution A and 5% BSA for 6 hours
470 at room temperature. Cubes were washed with 5 changes of solution A and
471 incubated at 4°C overnight.
472
473 Agarose samples were prepared for resin embedding, sectioned, and stained with
474 2% uranyl acetate and 1% lead citrate before imaging on a FEI Tecnai Biotwin
475 scope at 48k, 80kV.
476
477 **Reconstitution of endocytosis in PTK2 Cells:**

478 PTK2 cells were transfected to express palmitoylated GFP and cultured for 48
479 hours in a Mattek dish to confluence. Membrane sheets were prepared by
480 sonication, using 20% output power, 1 brief pulse on the center of the well. The
481 sheets were washed gently with cytosolic buffer and used within 20 min. The
482 membranes were incubated for 0, 5, 15, 30 min with a mix of 2 mg/ml cytosol, 1.5
483 mM ATP, ATP reconstitution system (16.7mM phosphocreatine,16.7U/ml creatine
484 phosphokinase), and 150 μM GTPγS. The reaction was stopped by gently wash 2
485 times with cytosolic buffer and immediately fixed with 4% PFA for 15min in PBS.
486 Membrane-bound proteins were detected using appropriate primary and
487 secondary antibodies. The membrane sheets were covered with cytosolic buffer.
488 Z stack images were captured using spinning disc confocal microscopy and
489 analyses were performed in ImageJ using Fiji. Z slices were summed to create a
490 single image. For each circular structure observed on membranes of interest,
491 linear ROIs were created and analyzed for size and fluorescence intensity.
492
493 **Isolation of synaptic membranes:**
494 All steps were executed at 4°C. Two wildtype mouse brains were washed in Buffer
495 A (1 mM $MgCl_2$, 1 mM $CaCl_2$, 1 mM $NaHCO_3$, 0.32 M sucrose) for 30 seconds and
496 transferred to a 55 mL potter homogenizer with 6 mL of Buffer A. The samples
497 were homogenized at 5,000 rpm for 10 strokes. The homogenate was centrifuged
498 at 1,400 x g for 10 min. Supernatant was retained. The pellet was resuspended in
499 6 mL of Buffer A and centrifuged at 700 x g for 10 min. Both supernatants were
500 combined and centrifuged at 17,500 x g for 15 min. The supernatant was
501 discarded, and the pellet was resuspended in 3 mL Buffer A. The resuspended
502 pellet (1.5 mL) was added to the top of freshly prepared 0.65 M, 0.85 M, 1.00 M,
503 1.20 M sucrose gradients (1.5 mL each concentration). The gradients were
504 centrifuged at 100,000 x g for 2 hours. Synaptosomes were collected from the
505 1/1.2 M interface and suspended in an excess of Buffer A. The synaptosomes were
506 centrifuged at 100,000 x g for 20 min. The pellet was resuspended in 4 mL ice-
507 cold deionized water, and HEPES pH 7.4 was added to a final concentration of
508 7.5mM. The suspension was incubated on ice for 30 min and centrifuged at
509 100,000 x g for 20 min. The pellet was resuspended in 4 mL of 0.1 M Na_2CO_3 to
510 strip peripheral proteins, incubated for 15 min at 37°C, and centrifuged at 100,000
511 x g for 20 min. Pellet was resuspended in 2 mL cytosolic buffer, centrifuged again
512 at 100,000 x g for 20 min, and resuspended in 2 mL cytosolic buffer. Proteins were
513 quantified using BCA bioassay. Mini cOmplete protease inhibitor cocktail was
514 added, and 100 μl aliquots of purified membrane resuspension were flash frozen
515 in liquid nitrogen and stored at -80°C.
516
517 **Cytosol purification:**
518 Mouse brains were removed and washed in washing buffer (23 mM Tris-HCl, pH
519 7.4, 320 mM sucrose) for 30 seconds. Two brains were homogenized at 2,500 rpm
520 in a 5 mL potter homogenizer with 2 mL of homogenization buffer (25mM Tris-HCl,
521 pH 8.0, 500 mM KCl, 250 mM sucrose, 2 mM EGTA, and 1 mM DTT), using 10
522 strokes at 5,000 rpm. The homogenate was transferred to a 3.5 mL ultracentrifuge
523 tube and centrifuged at 160,000 x g for 2 hours at 4°C. A PD-10 column was

524 equilibrated with 25 mL cytosolic buffer, the supernatant was added to the PD-10
525 column, and then, eluted with 3.5 mL of cytosolic buffer (25 mM Hepes-NaOH, pH
526 7.4, 120 mM potassium glutamate, 2.5 mM magnesium acetate, 20 mM KCl, and
527 5 mM EGTA-NaOH, pH 8.0, filtered and stored at 4°C, with 1 mM DTT added
528 immediately before use). Protein concentration was quantified by BSA assay. Mini
529 cOmplete protease inhibitor cocktail was added, and 100 μl aliquots were flash
530 frozen in liquid nitrogen and stored at -80°C.
531
532 **Synaptic membrane protein recruitment:**
533 Synaptic membranes (400 μg/mL) were mixed with 0.5 mg/mL wildtype or αβγ-
534 synuclein KO cytosolic proteins in 500 μl cytosolic buffer (see above, with 1 mM
535 DTT added immediately before use) and supplemented with an ATP regenerating
536 system (1.5 mM ATP, 16.7 mM phosphocreatine, and 16.7 U/mL creatine
537 phosphokinase) and 150 μM GTPγS. A control experiment was prepared with 400
538 μg/mL synaptic membranes in 500μl of cytosolic buffer alone. Mixtures were
539 pipetted 3 times to mix and incubated at 37°C for 15 min. The samples were
540 immediately centrifuged at 100,000 x g for 30 min at 4°C. Pellets were thoroughly
541 resuspended in 500 μl of cytosolic buffer at 4°C. The resuspension was centrifuged
542 at 100,000 x g for 30 min at 4° resuspended in 45 μl of cytosolic buffer. For each
543 sample, 20 μl aliquots were mixed with 5 μl of 5X loading buffer. Wildtype and αβγ-
544 synuclein knockout cytosol reference samples were prepared by diluting 32 μg of
545 each cytosol to 20 μl with cytosolic buffer and mixing with 5 μl of 5X loading buffer.
546 Samples were boiled for 10 min at 100°C. Levels of various proteins were
547 measured for each condition by quantitative immunoblotting.
548
549 **Reconstitution of clathrin recruitment on lipid monolayers:**
550
551 *Purification of proteins*
552 α-Synuclein and AP180 were recombinantly expressed and purified from BL21
553 (DE3) *E. Coli* as previously described [24, 30, 58]. Clathrin was purified from
554 porcine or bovine brains by purifying CCVs and disassembling cages as described
555 [59]. For the described experiments, we used porcine and bovine clathrin
556 interchangeably with no significant difference.
557
558 *Lipid Monolayer Assay with Purified Proteins*
559 An 8-well Teflon block was arranged in a humid chamber and wells were filled with
560 40-60 μL of HKM buffer (25 mM HEPES pH 7.4, 125 mM potassium acetate, 5mM
561 magnesium acetate, 1mM dithiothreitol). Lipid mixture (10% cholesterol, 40% PE,
562 40% PC, and 10% PI(4,5)P2 to final concentration of 0.1 mg/mL in a 19:1 mixture
563 of chloroform to methanol) was carefully pipetted onto the buffer in each well. The
564 blocks were incubated in a humid chamber at room temperature for 1 hour to
565 evaporate methanol/chloroform. Carbon-coated copper grids were placed carbon-
566 side down onto each well. Proteins were introduced via side-injection ports beside
567 each well. Final protein concentrations per well were as follows: 2 μM AP180 and
568 α-synuclein, 500 nM purified bovine/porcine clathrin. Grids were incubated for 60

min in a humid chamber at room temperature, and then, removed from the block and immediately negative stained with 1% uranyl acetate. After drying, grids were imaged on a Phillip CM10 transmission electron microscope at 46k, 80kV). Clathrin lattices were outlined manually and the areas were quantified in Image J. Non-hexagonal clathrin lattices could not be quantified due to the high contrast needed to visualize these structures in these experiments.

Lipid Monolayer Assay with Mouse Brain Cytosol

5 mg/mL wild type and αβγ-synuclein KO mouse brain cytosol was added to wells of the Teflon block. Lipid mixture (see above) was pipetted on top of the cytosol. Blocks were incubated in a humid chamber for 1 hour to evaporate methanol/chloroform. Carbon-coated copper grids were placed on top of the wells, and an ATP regenerating system (see above) and 150 μM GTPγS were introduced through a side injection port. Grids were incubated in a humid chamber at 37˚C for 0, 5, 15, or 30 min and then removed from the block and immediately negative stained as described above. Grids were imaged on a FEI Tecnai Biotwin at scope 42k, 80kV. Clathrin lattices were outlined manually, the area and number of pentagons, heptagons and hexagons were quantified in Image J.

Crosslinking experiments:

Synaptosomes were isolated from wildtype and αβγ-synuclein KO mouse brains as described. Synaptosomes were incubated with SDAD crosslinker (1 mM; Thermo) or DMSO as control and incubated on ice for 45 minutes. The reaction was stopped with 100 μl 1M Tris, pH 8.0 on ice for 15 minutes. The excess crosslinker was removed by centrifugation. The synaptosomes were then UV crosslinked for 1 minute with a Strategene UV light (254 nm). Crosslinked synaptic membranes were solubilized with 1% Triton and used as starting material for α-synuclein immunoprecipitation experiments. The immunoprecipitants were run on SDS-PAGE, silver stained with a mass spectrometry compatible silver stain (Pierce), relevant bands were excised and identified by LC-MS.

Statistics:

All experimental analysis was done blinded to condition. Statistical analysis was performed by GraphPad. Data is presented as average ± SEM.

Acknowledgments: This work was supported by NIH (R01 NS064963, R01 NS110354, R01 NS083846), Nina Compagnon Hirshfield Parkinson's Disease Research Fund and DOD (W81XWH-17-1-0564). The proteomic experiments were supported by the NIDA Neuroproteomic Center (NIH DA018343-11A1). We would like to thank Dr. Pietro De Camilli and his lab members for Dynamin1,3 double KO pups as well as help in performing the PTK2 cell assays. We thank Aurelie Nardin for setting up the PTK2 assay, Christopher Westphal and Becket Greten-Harrison for help with cross-linking experiments. We thank John. E. Lee for editing the manuscript.

615 **Author contributions:** KJV, PC and SSC designed research/experiments; KJV,
616 PC, EG and SSC performed experiments; KJV, PC, EG and SSC analyzed data;
617 All authors wrote and edited the paper.
618
619 **Figure Legends**
620
621 **Figure 1. α-Synuclein localization is dynamically regulated by neuronal**
622 **activity.** (**A**) Electron micrographs of permeabilized synaptosomes at rest,
623 stimulated with 90 mM KCl, and upon recovery. Immuno-gold labeled α-synuclein
624 is localized to SVs at rest (arrowhead). During stimulation, α-synuclein
625 disassociates from SVs and predominantly localizes on the synaptic membrane.
626 During recovery, α-synuclein returns to the SV membrane. (**B**) Electron
627 micrographs of permeabilized synaptosomes in rest, stimulation, and recovery
628 conditions immuno-labeled for synaptobrevin2. Gold-labeled synaptobrevin 2
629 remains associated with the vesicle in all three conditions. (**C-D**) Quantification of
630 gold label localization for α-synuclein and synaptobrevin2. Bars represent percent
631 gold label from n=3 independent experiments for control conditions and n=2 for
632 remaining conditions. 25-40 micrographs per condition were analyzed. ANOVA
633 was used to determine significance. * $p<0.05$; ** $p<0.01$ and *** $p<0.0001$. Scale
634 bar=100 nm.
635
636 **Figure 2. α-Synuclein and clathrin co-localize in patches on the plasma**
637 **membrane.** (**A**) Membrane sheets from PTK2 cells immunostained for α-synuclein
638 (red) and clathrin heavy chain (green). α-Synuclein and clathrin are present in
639 patches on the membrane, with some patches containing both proteins. Scale bar=
640 1 μm. (**B**) Zoomed-in view of a clathrin+α-synuclein patch. Note that α-synuclein
641 localizes to the center of the clathrin patch. (**C**) α-Synuclein only patches, which
642 are on average smaller than clathrin patches. (**D**) Plot of fluorescence of clathrin
643 versus α-synuclein colored by size of the clathrin patch. The dashed lines (x=0.5
644 and y=1) indicate the cut-offs used to demarcate patches into clathrin only ($x<0.5$,
645 $y>1$), α-synuclein only ($x>0.5$, $y<1$), and clathrin+α-synuclein ($x>0.5$, $y>1$) puncta.
646 Plots show that colocalization of clathrin and α-synuclein is predominant in larger
647 size patches. (**E**) Intensity of clathrin and α-synuclein in different patch sizes. (**F**)
648 Average size of clathrin only, α-synuclein only and clathrin+α-synuclein patches.
649 (**G**) Changes in the three population of patches over the time when incubated with
650 wildtype purified cytosol. N=3 independent experiments. * $p<0.05$; ** $p<0.01$ and
651 *** $p<0.0001$. Scale bar=1 μm.
652
653 **Figure 3. Recruitment of endocytic proteins to synaptic membranes from**
654 **wildtype and αβγ-synuclein KO brain cytosol.** (**A-B**) Western blot of endocytic
655 proteins recruited from wildtype (WT) and αβγ-synuclein KO (TKO) cytosol to
656 synaptic membranes (Recruitment). Membrane fraction without addition of cytosol
657 is used as a control. N-cadherin was used as a membrane loading control.
658 Abbreviations: Memb, synaptic membrane fraction; CLC, clathrin light chain; CHC,
659 clathrin heavy chain; AAK1, AP2 Associated Kinase-1. (**C**) Quantification of
660 membrane recruitment of endocytic proteins. Western blot quantifications (n=3

661 independent experiments) after normalizing for added membranes (N-Cadherin
662 signal). * $p<0.05$, ** $p<0.01$, Student's t-test.
663
664 **Figure 4. Lipid monolayer assay to visualize clathrin recruitment from brain**
665 **cytosol.** (**A**) Schematic of Teflon block and experimental setup used in monolayer
666 reconstitutions. Wells (W) and Side Injection Ports (SIP) labeled. (**B**) Electron
667 micrographs showing the clathrin assembly into flat lattices and CCPs on
668 membrane monolayers over time (0,15, 23, and 30 min). These monolayers were
669 incubated with cytosol from wild type (WT), αβγ-synuclein KO (TKO), and mouse
670 α-synuclein added to TKO cytosol (rescue). Clathrin patches are highlighted with
671 red outlines. Arrow indicates CCP. N=3 independent experiments with 10 images
672 per experiment. Scale bar=100 nm. (**C**) Comparison of clathrin patch areas in the
673 three conditions mentioned above. (**D**) Examples of pentagon, hexagon and
674 heptagon clathrin lattices. (**E**) Ratio of non-hexagons (pentagons and heptagons)
675 to hexagon in clathrin lattices for each of the three conditions, t=23 min. (**F**)
676 Histogram of non-hexagon to hexagon ratio for the three conditions. The sum of
677 all weights was used to normalize the data. For all graphs: * $p<0.05$; ** $p<0.01$ and
678 *** $p<0.0001$. Welsh's t-test.
679
680 **Figure 5. Reconstitution of clathrin assembly using recombinant proteins.**
681 (**A**) Coomassie stain showing proteins used in reconstitution conditions. (**B**)
682 Electron micrographs of negative controls. Left: Lipid monolayer with no added
683 protein. Center: recombinant AP180 added to lipid monolayer. Right: Brain purified
684 clathrin added to lipid monolayer. Lower: All proteins without a lipid monolayer
685 Under all four conditions no clathrin cages form. (**C-E**) Electron micrographs of
686 constituent proteins added to lipid monolayers. (**C**) Left: Recombinant wildtype
687 mouse α-synuclein. Only membrane ruffles are observed. Center Recombinant
688 mouse AP180 and α-synuclein. Left: α-Synuclein and isolated clathrin added to
689 lipid monolayer. (**D**) Electron micrographs of clathrin and AP180 added to lipid
690 monolayer. Characteristic fullerene-shaped clathrin cages form. Inset: Zoomed
691 image outlined in green (**E**) Electron micrographs of α-synuclein, clathrin, and
692 AP180 added to lipid monolayer. Inset: Zoomed image outlined in blue. Scale bar
693 = 200 nm. (**F**) Quantification of area of clathrin patches obtained in conditions **D**
694 and **E**. Addition of α-synuclein increases the area of clathrin patches. N=3
695 independent experiments with at least 10 micrographs per experiment. * $p<0.05$;
696 ** $p<0.01$ and *** $p<0.0001$. Scale bar=100 nm.
697
698

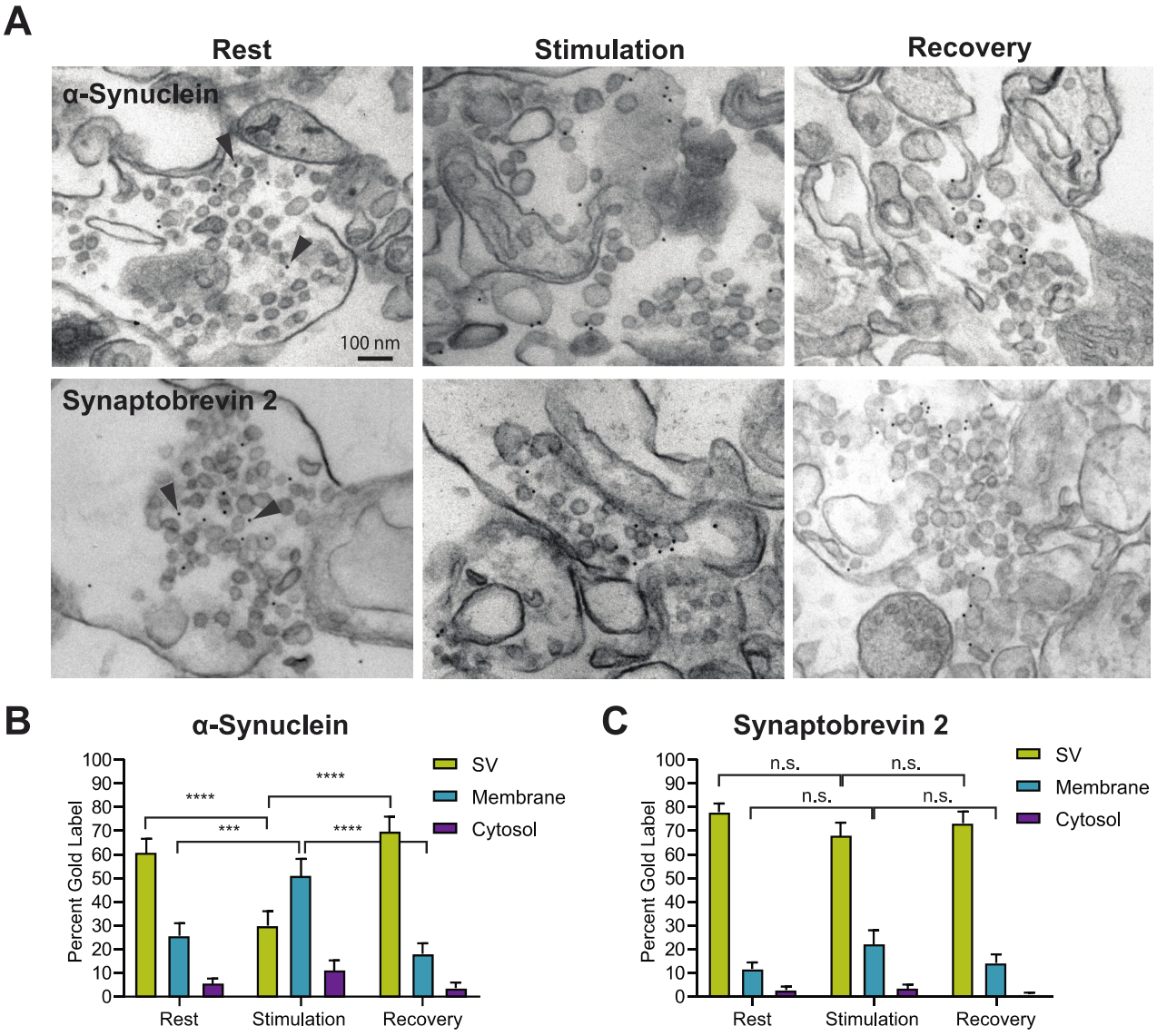
A
Rest
Stimulation
Recovery
α-Synuclein
100 nm
Synaptobrevin 2
B
α-Synuclein
Percent Gold Label
SV
Membrane
Cytosol
****
***
****
****
Rest
Stimulation
Recovery
C
Synaptobrevin 2
n.s.
n.s.
n.s.
n.s.

Figure 1

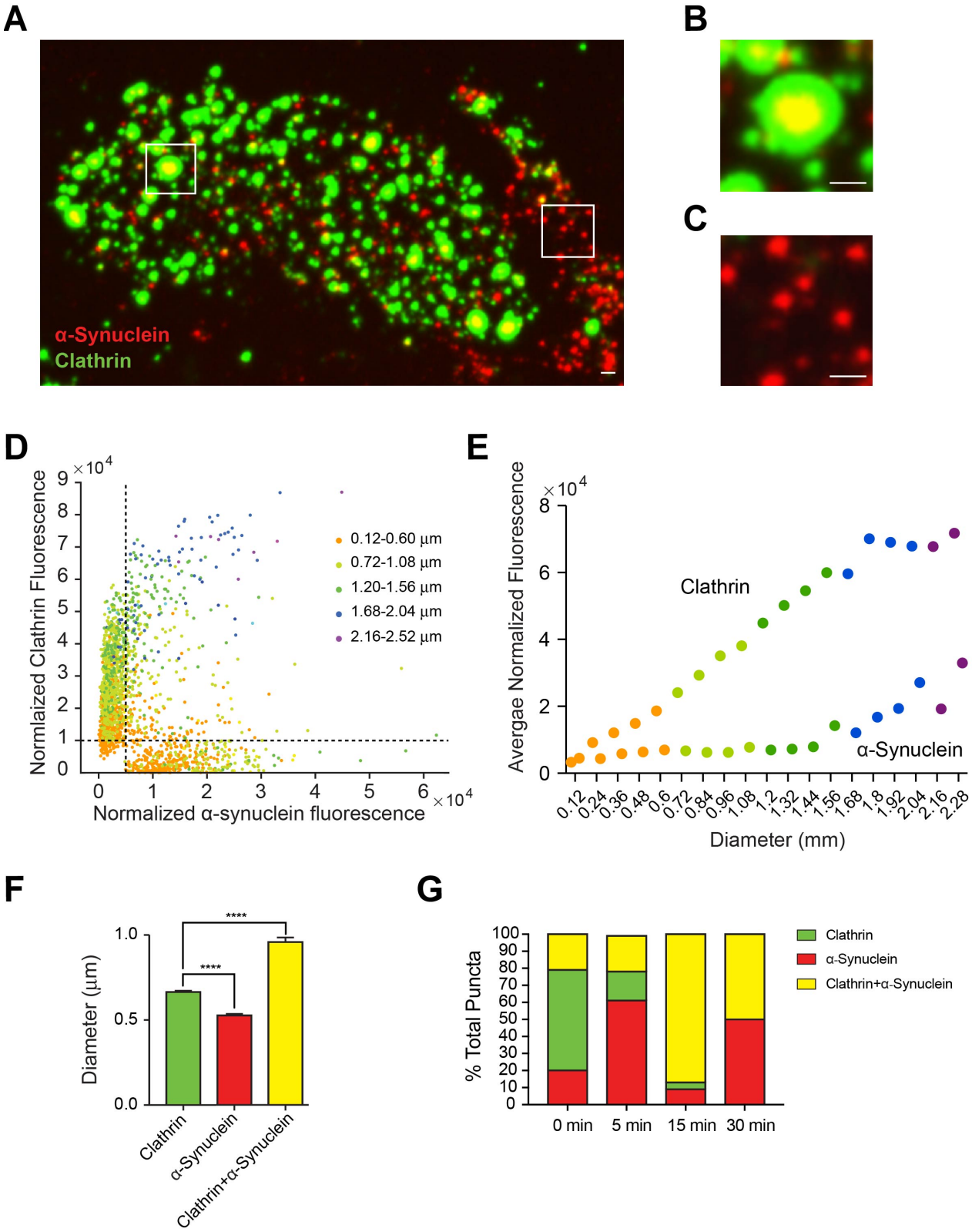
A
α-Synuclein
Clathrin
B
C
D
Normlaized Clathrin Fluorescence
Normalized α-synuclein fluorescence
0.12-0.60 µm
0.72-1.08 µm
1.20-1.56 µm
1.68-2.04 µm
2.16-2.52 µm
E
Avergae Normalized Fluorescence
Clathrin
α-Synuclein
Diameter (mm)
F
Diameter (µm)
Clathrin
α-Synuclein
Clathrin+α-Synuclein
G
% Total Puncta
0 min
5 min
15 min
30 min
Clathrin
α-Synuclein
Clathrin+α-Synuclein

Figure 2

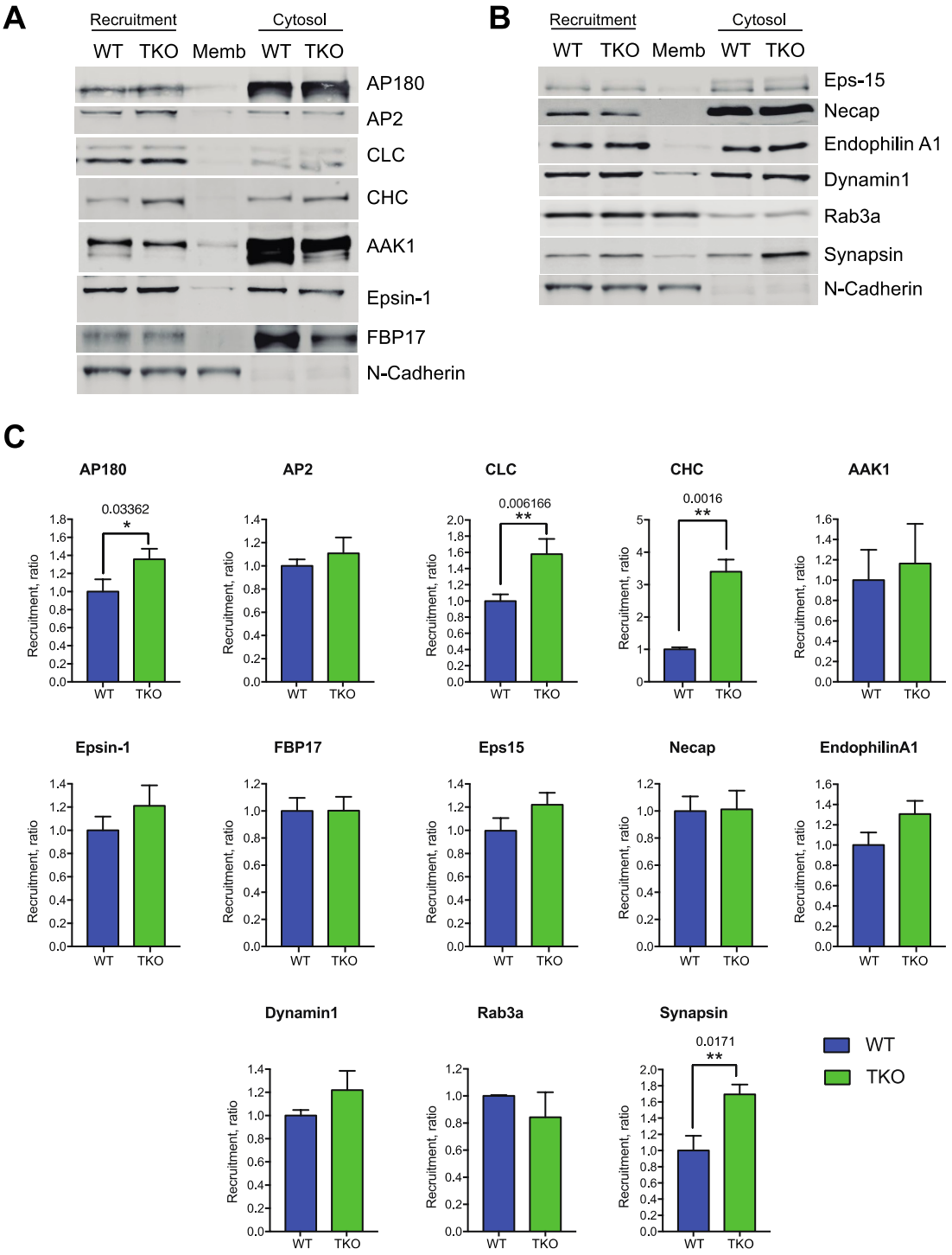
A
Recruitment
Cytosol
WT TKO Memb WT TKO
AP180
AP2
CLC
CHC
AAK1
Epsin-1
FBP17
N-Cadherin
B
Recruitment
Cytosol
WT TKO Memb WT TKO
Eps-15
Necap
Endophilin A1
Dynamin1
Rab3a
Synapsin
N-Cadherin
C
AP180
0.03362
*
AP2
CLC
0.006166
**
CHC
0.0016
**
AAK1
Epsin-1
FBP17
Eps15
Necap
EndophilinA1
Dynamin1
Rab3a
Synapsin
0.0171
**
Recruitment, ratio
WT
TKO

Figure 3

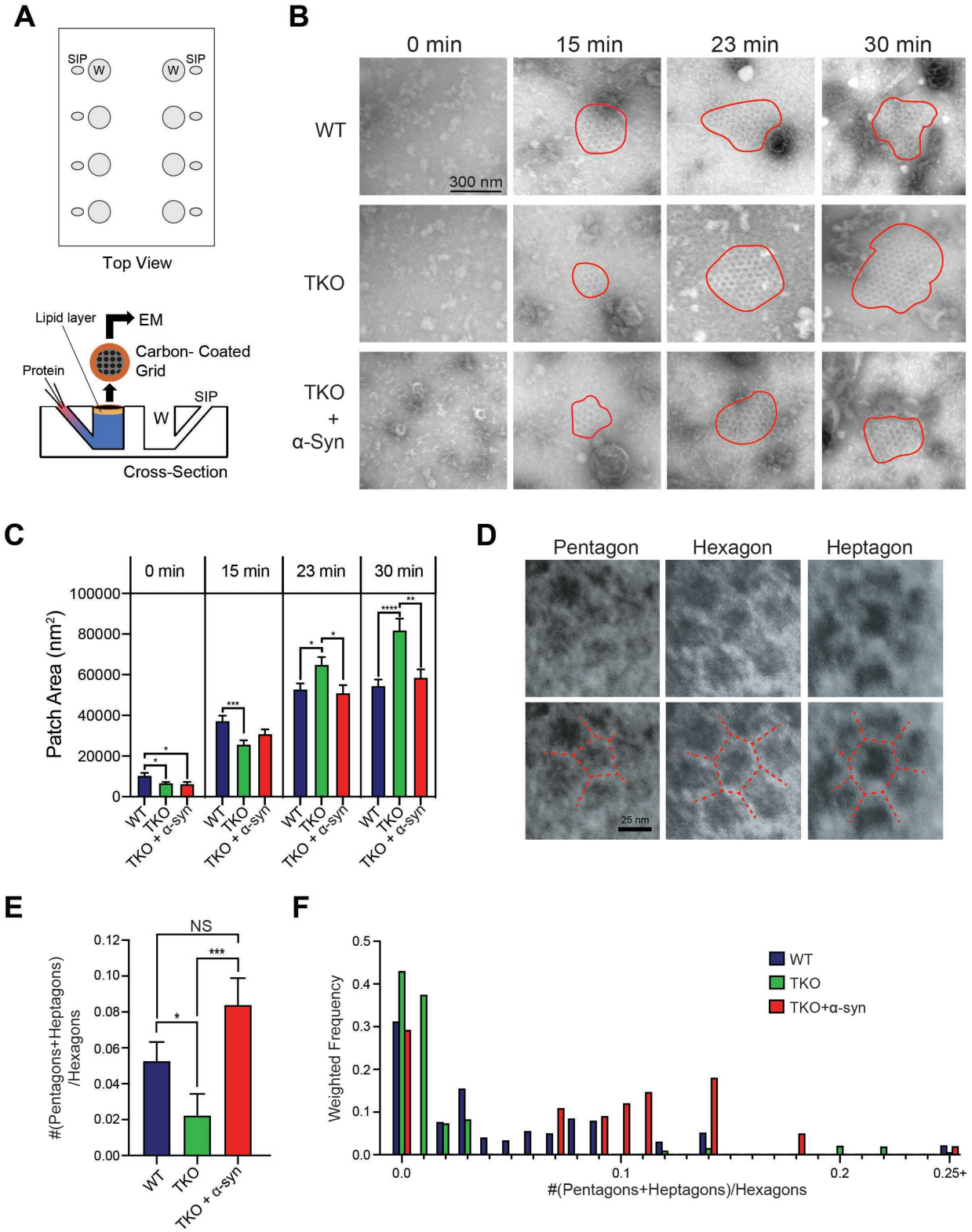
A
SIP
W
W
SIP
Top View
Lipid layer
EM
Carbon- Coated Grid
Protein
SIP
W
Cross-Section
B
0 min
15 min
23 min
30 min
WT
TKO
TKO + α-Syn
300 nm
C
0 min
15 min
23 min
30 min
Patch Area (nm²)
100000
80000
60000
40000
20000
0
WT
TKO
TKO + α-syn
D
Pentagon
Hexagon
Heptagon
25 nm
E
NS
***
*
#(Pentagons+Heptagons) /Hexagons
0.12
0.10
0.08
0.06
0.04
0.02
0.00
WT
TKO
TKO + α-syn
F
WT
TKO
TKO+α-syn
Weighted Frequency
0.5
0.4
0.3
0.2
0.1
0.0
0.0
0.1
0.2
0.25+
#(Pentagons+Heptagons)/Hexagons

Figure 4

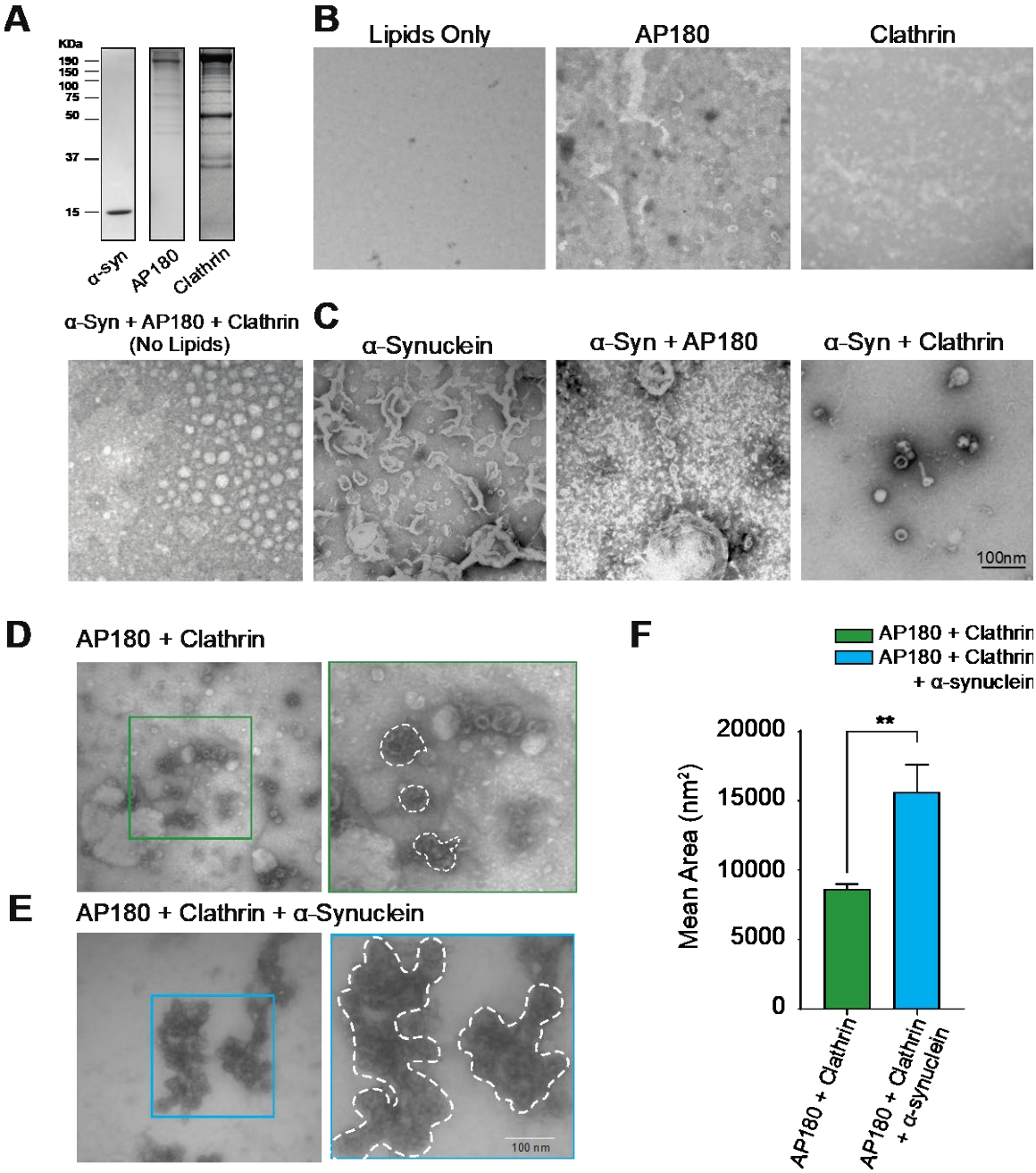
A
KDa
190
150
100
75
50
37
15
α-Syn
AP180
Clathrin
B
Lipids Only
AP180
Clathrin
α-Syn + AP180 + Clathrin
(No Lipids)
C
α-Synuclein
α-Syn + AP180
α-Syn + Clathrin
100nm
D
AP180 + Clathrin
E
AP180 + Clathrin + α-Synuclein
100 nm
F
AP180 + Clathrin
AP180 + Clathrin
+ α-synuclein
**
Mean Area (nm²)
20000
15000
10000
5000
0
AP180 + Clathrin
AP180 + Clathrin
+ α-synuclein

Figure 5

SUPPLEMENTARY FIGURES

Title: α-Synuclein facilitates clathrin assembly in synaptic vesicle endocytosis

Short title: α-Synuclein regulates clathrin assembly

Karina J Vargas[1*#], P. L. Colosi[1,2*#], Eric Girardi[1*], Sreeganga S Chandra[1,3]

[1] Departments of Neurology; Neuroscience, Yale University, New Haven, CT 06536
[2] PREP Program, Yale University, New Haven, CT 06511
[3] To whom correspondence should be addressed to:
sreeganga.chandra@yale.edu ; 203-785-6172

*Authors contributed equally to this study
Present Address:
KJV, Marine Biological Laboratory, MA
PLC, University of Pennsylvania, PA

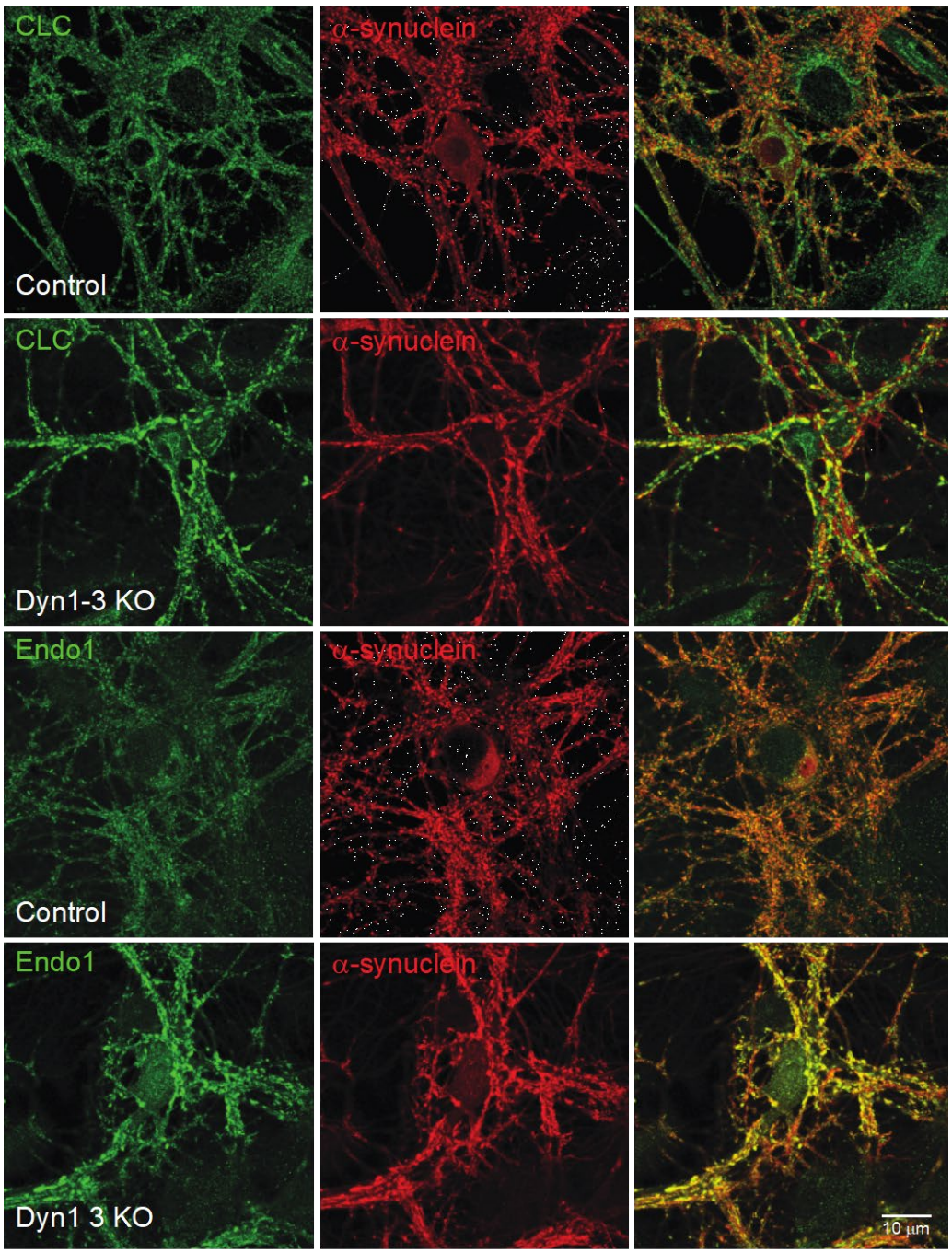

Supplementary Figure 1. α-Synuclein is localized to endocytic clusters in Dynamin1,3 double KO neurons. Control and Dynamin1,3 double KO neurons were immunostained with antibodies to an endocytic protein (clathrin-CLC or Endophilin A1-Endo1) and α-synuclein. Clustering of endocytic proteins is observed in the Dynamin1,3 double KO but not in the Control. α-Synuclein colocalizes with other trapped endocytic proteins. Scale bar =10 um.

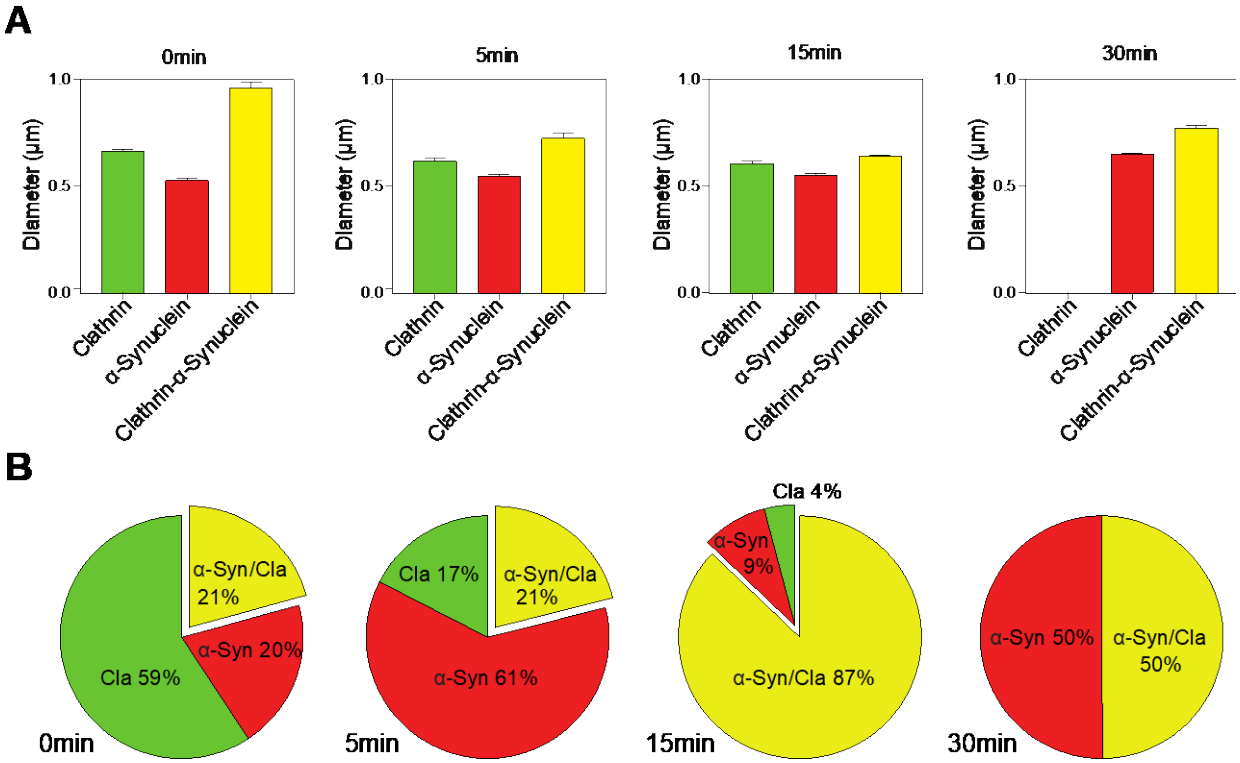

Supplementary Figure 2. Temporal changes of size and colocalization of α-synuclein and clathrin patches. PTK2 cells were sheared and processed to detect α-synuclein and clathrin on the resulting membrane sheets. **(A)** Size comparisons of clathrin only, α-synuclein only, and clathrin+α-synuclein patches at the denoted time points. Welsh's t-test was used to determine significance. * $p<0.05$; ** $p<0.01$ and *** $p<0.0001$. **(B)** Fraction of the three type of patches as a function of time.

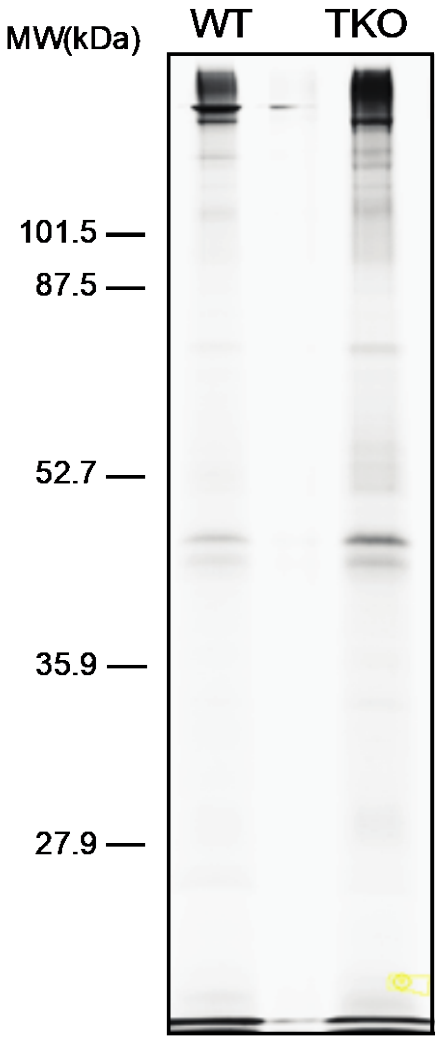

Supplementary Figure 3. Immunoprecipitation of crosslinked α-synuclein from wild type and αβγ-synuclein KO synaptosomes. Wild type (WT) and αβγ-synuclein KO (TKO) synaptosomes were crosslinked, solubilized and immunoprecipitated with an antibody against α-synuclein. The immunoprecipitants were load in a polyacrylamide gel and stained with silver. Bands marked with boxes were cut and processed for mass spectroscopy.

References

1. Spillantini, M.G., et al., *Alpha-synuclein in Lewy bodies.* Nature, 1997. **388**(6645): p. 839-40.
2. Ferese, R., et al., *Four Copies of SNCA Responsible for Autosomal Dominant Parkinson's Disease in Two Italian Siblings.* Parkinsons Dis, 2015. **2015**: p. 546462.
3. Ibanez, P., et al., *Causal relation between alpha-synuclein gene duplication and familial Parkinson's disease.* Lancet, 2004. **364**(9440): p. 1169-71.
4. Kruger, R., et al., *Ala30Pro mutation in the gene encoding alpha-synuclein in Parkinson's disease.* Nat Genet, 1998. **18**(2): p. 106-8.
5. Polymeropoulos, M.H., et al., *Mutation in the alpha-synuclein gene identified in families with Parkinson's disease.* Science, 1997. **276**(5321): p. 2045-7.
6. Singleton, A.B., et al., *alpha-Synuclein locus triplication causes Parkinson's disease.* Science, 2003. **302**(5646): p. 841.
7. Zarranz, J.J., et al., *The new mutation, E46K, of alpha-synuclein causes Parkinson and Lewy body dementia.* Ann Neurol, 2004. **55**(2): p. 164-73.
8. Satake, W., et al., *Genome-wide association study identifies common variants at four loci as genetic risk factors for Parkinson's disease.* Nat Genet, 2009. **41**(12): p. 1303-7.
9. Simon-Sanchez, J., et al., *Genome-wide association study reveals genetic risk underlying Parkinson's disease.* Nat Genet, 2009. **41**(12): p. 1308-12.
10. Maroteaux, L., J.T. Campanelli, and R.H. Scheller, *Synuclein: a neuron-specific protein localized to the nucleus and presynaptic nerve terminal.* J Neurosci, 1988. **8**(8): p. 2804-15.
11. Lokappa, S.B. and T.S. Ulmer, *Alpha-synuclein populates both elongated and broken helix states on small unilamellar vesicles.* J Biol Chem, 2011. **286**(24): p. 21450-7.
12. Ferreon, A.C., et al., *Interplay of alpha-synuclein binding and conformational switching probed by single-molecule fluorescence.* Proc Natl Acad Sci U S A, 2009. **106**(14): p. 5645-50.
13. Middleton, E.R. and E. Rhoades, *Effects of curvature and composition on alpha-synuclein binding to lipid vesicles.* Biophys J, 2010. **99**(7): p. 2279-88.
14. Burre, J., M. Sharma, and T.C. Sudhof, *alpha-Synuclein assembles into higher-order multimers upon membrane binding to promote SNARE complex formation.* Proc Natl Acad Sci U S A, 2014. **111**(40): p. E4274-83.
15. Burre, J., et al., *Alpha-synuclein promotes SNARE-complex assembly in vivo and in vitro.* Science, 2010. **329**(5999): p. 1663-7.
16. Sun, J., et al., *Functional cooperation of alpha-synuclein and VAMP2 in synaptic vesicle recycling.* Proc Natl Acad Sci U S A, 2019. **116**(23): p. 11113-11115.
17. Diao, J., et al., *Native alpha-synuclein induces clustering of synaptic-vesicle mimics via binding to phospholipids and synaptobrevin-2/VAMP2.* Elife, 2013. **2**: p. e00592.
18. Greten-Harrison, B., et al., *alphabetagamma-Synuclein triple knockout mice reveal age-dependent neuronal dysfunction.* Proc Natl Acad Sci U S A, 2010. **107**(45): p. 19573-8.

745 19. Anwar, S., et al., *Functional alterations to the nigrostriatal system in mice*
746 *lacking all three members of the synuclein family.* J Neurosci, 2011. **31**(20): p.
747 7264-74.
748 20. Vargas, K.J., et al., *Synucleins regulate the kinetics of synaptic vesicle*
749 *endocytosis.* J Neurosci, 2014. **34**(28): p. 9364-76.
750 21. Vargas, K.J., et al., *Synucleins Have Multiple Effects on Presynaptic Architecture.*
751 Cell Rep, 2017. **18**(1): p. 161-173.
752 22. Logan, T., et al., *alpha-Synuclein promotes dilation of the exocytotic fusion*
753 *pore.* Nat Neurosci, 2017. **20**(5): p. 681-689.
754 23. Atias, M., et al., *Synapsins regulate alpha-synuclein functions.* Proc Natl Acad
755 Sci U S A, 2019. **116**(23): p. 11116-11118.
756 24. Westphal, C.H. and S.S. Chandra, *Monomeric synucleins generate membrane*
757 *curvature.* J Biol Chem, 2013. **288**(3): p. 1829-40.
758 25. Chung, C.Y., et al., *In Situ Peroxidase Labeling and Mass-Spectrometry Connects*
759 *Alpha-Synuclein Directly to Endocytic Trafficking and mRNA Metabolism in*
760 *Neurons.* Cell Syst, 2017. **4**(2): p. 242-250 e4.
761 26. Burre, J., M. Sharma, and T.C. Sudhof, *Systematic mutagenesis of alpha-*
762 *synuclein reveals distinct sequence requirements for physiological and*
763 *pathological activities.* J Neurosci, 2012. **32**(43): p. 15227-42.
764 27. Koo, S.J., D. Puchkov, and V. Haucke, *AP180 and CALM: Dedicated endocytic*
765 *adaptors for the retrieval of synaptobrevin 2 at synapses.* Cell Logist, 2011.
766 **1**(4): p. 168-172.
767 28. Moshkanbaryans, L., L.S. Chan, and M.E. Graham, *The Biochemical Properties*
768 *and Functions of CALM and AP180 in Clathrin Mediated Endocytosis.*
769 Membranes (Basel), 2014. **4**(3): p. 388-413.
770 29. Koo, S.J., et al., *Vesicular Synaptobrevin/VAMP2 Levels Guarded by AP180*
771 *Control Efficient Neurotransmission.* Neuron, 2015. **88**(2): p. 330-44.
772 30. Ford, M.G., et al., *Simultaneous binding of PtdIns(4,5)P2 and clathrin by AP180*
773 *in the nucleation of clathrin lattices on membranes.* Science, 2001. **291**(5506):
774 p. 1051-5.
775 31. Miller, S.E., et al., *CALM regulates clathrin-coated vesicle size and maturation*
776 *by directly sensing and driving membrane curvature.* Dev Cell, 2015. **33**(2): p.
777 163-75.
778 32. Qualmann, B., D. Koch, and M.M. Kessels, *Let's go bananas: revisiting the*
779 *endocytic BAR code.* EMBO J, 2011. **30**(17): p. 3501-15.
780 33. Ferguson, S.M., et al., *A selective activity-dependent requirement for dynamin 1*
781 *in synaptic vesicle endocytosis.* Science, 2007. **316**(5824): p. 570-4.
782 34. Clayton, D.F. and J.M. George, *Synucleins in synaptic plasticity and*
783 *neurodegenerative disorders.* J Neurosci Res, 1999. **58**(1): p. 120-9.
784 35. Antonny, B., *Mechanisms of membrane curvature sensing.* Annu Rev Biochem,
785 2011. **80**: p. 101-23.
786 36. Rhoades, E., et al., *Quantification of alpha-synuclein binding to lipid vesicles*
787 *using fluorescence correlation spectroscopy.* Biophys J, 2006. **90**(12): p. 4692-
788 700.
789 37. Fortin, D.L., et al., *Neural activity controls the synaptic accumulation of alpha-*
790 *synuclein.* J Neurosci, 2005. **25**(47): p. 10913-21.

791 38. Wang, L., et al., *alpha-synuclein multimers cluster synaptic vesicles and*
792 *attenuate recycling.* Curr Biol, 2014. **24**(19): p. 2319-26.
793 39. Raimondi, A., et al., *Overlapping role of dynamin isoforms in synaptic vesicle*
794 *endocytosis.* Neuron, 2011. **70**(6): p. 1100-14.
795 40. Wu, M., et al., *Coupling between clathrin-dependent endocytic budding and F-*
796 *BAR-dependent tubulation in a cell-free system.* Nat Cell Biol, 2010. **12**(9): p.
797 902-8.
798 41. Hosaka, M., R.E. Hammer, and T.C. Sudhof, *A phospho-switch controls the*
799 *dynamic association of synapsins with synaptic vesicles.* Neuron, 1999. **24**(2):
800 p. 377-87.
801 42. Chandra, S., et al., *Alpha-synuclein cooperates with CSPalpha in preventing*
802 *neurodegeneration.* Cell, 2005. **123**(3): p. 383-96.
803 43. Bucher, D., et al., *Clathrin-adaptor ratio and membrane tension regulate the*
804 *flat-to-curved transition of the clathrin coat during endocytosis.* Nat Commun,
805 2018. **9**(1): p. 1109.
806 44. Evergren, E., et al., *A pre-embedding immunogold approach for detection of*
807 *synaptic endocytic proteins in situ.* J Neurosci Methods, 2004. **135**(1-2): p.
808 169-74.
809 45. Pechstein, A., et al., *Regulation of synaptic vesicle recycling by complex*
810 *formation between intersectin 1 and the clathrin adaptor complex AP2.* Proc
811 Natl Acad Sci U S A, 2010. **107**(9): p. 4206-11.
812 46. Ringstad, N., et al., *Endophilin/SH3p4 is required for the transition from early*
813 *to late stages in clathrin-mediated synaptic vesicle endocytosis.* Neuron, 1999.
814 **24**(1): p. 143-54.
815 47. Sochacki, K.A., et al., *Endocytic proteins are partitioned at the edge of the*
816 *clathrin lattice in mammalian cells.* Nature Cell Biology, 2017. **19**(4): p. 352-+.
817 48. Busch, D.J., et al., *Acute increase of alpha-synuclein inhibits synaptic vesicle*
818 *recycling evoked during intense stimulation.* Mol Biol Cell, 2014. **25**(24): p.
819 3926-41.
820 49. Xu, J., et al., *alpha-Synuclein Mutation Inhibits Endocytosis at Mammalian*
821 *Central Nerve Terminals.* J Neurosci, 2016. **36**(16): p. 4408-14.
822 50. Nemani, V.M., et al., *Increased expression of alpha-synuclein reduces*
823 *neurotransmitter release by inhibiting synaptic vesicle reclustering after*
824 *endocytosis.* Neuron, 2010. **65**(1): p. 66-79.
825 51. Eguchi, K., et al., *Wild-Type Monomeric alpha-Synuclein Can Impair Vesicle*
826 *Endocytosis and Synaptic Fidelity via Tubulin Polymerization at the Calyx of*
827 *Held.* J Neurosci, 2017. **37**(25): p. 6043-6052.
828 52. Susan M. L. Banks, A.T.M., Molly McQuillan, David J. Busch, Ana Sofia
829 Ibarraran-Viniegra, Subhojit Roy, Rui Sousa, Eileen M. Lafer, Jennifer R.
830 Morgan, *Hsc70 Ameliorates the Vesicle Recycling Defects Caused by Excess α-*
831 *Synuclein at Synapses.* Neuroscience Online, 2020.
832 53. Cao, M., et al., *Parkinson Sac Domain Mutation in Synaptojanin 1 Impairs*
833 *Clathrin Uncoating at Synapses and Triggers Dystrophic Changes in*
834 *Dopaminergic Axons.* Neuron, 2017. **93**(4): p. 882-896 e5.
835 54. Cremona, O., et al., *Essential role of phosphoinositide metabolism in synaptic*
836 *vesicle recycling.* Cell, 1999. **99**(2): p. 179-88.

837 55. Yim, Y.I., et al., *Endocytosis and clathrin-uncoating defects at synapses of*
838 *auxilin knockout mice.* Proc Natl Acad Sci U S A, 2010. **107**(9): p. 4412-7.
839 56. Olgiati, S., et al., *DNAJC6 Mutations Associated With Early-Onset Parkinson's*
840 *Disease.* Ann Neurol, 2016. **79**(2): p. 244-56.
841 57. De Camilli, P., et al., *Synapsin I (Protein I), a nerve terminal-specific*
842 *phosphoprotein. II. Its specific association with synaptic vesicles demonstrated*
843 *by immunocytochemistry in agarose-embedded synaptosomes.* J Cell Biol, 1983.
844 **96**(5): p. 1355-73.
845 58. Taguchi, Y.V., et al., *Glucosylsphingosine Promotes alpha-Synuclein Pathology*
846 *in Mutant GBA-Associated Parkinson's Disease.* J Neurosci, 2017. **37**(40): p.
847 9617-9631.
848 59. Chen, Y., et al., *Dynamic instability of clathrin assembly provides proofreading*
849 *control for endocytosis.* J Cell Biol, 2019. **218**(10): p. 3200-3211.
850